Chemisorption Properties and Structural Evolution of Pt−Si Intermetallic Thin Films Prepared by the Activated Adsorption of SiH_4 on Pt(111)

Michael S. Nashner,† Joseph C. Bondos, Michael J. Hostetler,‡ Andrew A. Gewirth,* and Ralph G. Nuzzo*

School of Chemical Sciences and the Frederick Seitz Materials Research Laboratory, University of Illinois, Urbana, Illinois 61801

Received: March 10, 1998; In Final Form: May 12, 1998

The reaction of a silicon adlayer deposited on Pt(111) by chemical vapor deposition (CVD) using silane (SiH_4) is described. Data from Auger electron spectroscopy (AES) reveal that Si readily diffuses into the Pt substrate and sequentially forms at least two unique intermetallic Pt−Si surface structural phases with $(\sqrt{7} \times \sqrt{7})R19.1°$ and $(\sqrt{19} \times \sqrt{19})R23.4°$ real space unit cells as characterized by low-energy electron diffraction (LEED). The chemisorption properties of each of the ordered overlayers were studied using CO as a molecular probe. Reflection−absorption infrared spectroscopy (RAIRS) and temperature-programmed desorption (TPD) studies indicated that CO was mostly limited to chemisorption at "atop" Pt sites in the $\sqrt{7}$ phase with a significant reduction of the heat of adsorption with respect to the Pt(111) surface. The $\sqrt{19}$ phase also showed a significant modification of the chemisorption properties although it is not as pronounced as that seen for the $\sqrt{7}$ structure. The relevance of these studies to intermetallic thin film growth is discussed.

Introduction

Intermetallic thin films prepared via metal−semiconductor reactions are of fundamental importance in the microelectronics industry.[1,2] For example, transition-metal silicides have been widely used as interconnects, gates, and contacts (Schottky barrier and Ohmic) in very large scale integration (VLSI) device technology.[1−3] More recently, Pt−Si/Si Schottky diodes have emerged as promising new infrared detectors in the 3−5 μm wavelength range.[4] As device dimensions have decreased, the need to develop a better understanding of the structure, physical, and chemical properties of metal−semiconductor intermetallic thin films has become increasingly important. One key to understanding the nature of the thin-film reactions used to prepare these materials lies at the metal−silicon interface, where nonequilibrium phase behavior is strongly influenced by the interfacial reaction kinetics.[1−3,5−8]

Most solid−solid reaction studies of the metal−semiconductor interface involve the deposition of metal thin films (<1 μm) on semiconductor surfaces followed by various annealing treatments.[1−16] For example, annealing a thin film of Pt (∼100 nm) deposited on a silicon substrate at ca. 573 K results in the nucleation and growth of a uniform Pt_2Si phase even though the phase diagram indicates the existence of at least five stable phases for the Pt−Si system at the same temperature. We note that this temperature is significantly lower than the lowest eutectic in the bulk binary phase diagram. Only after depletion of the Pt_2Si will the thermodynamically-preferred silicon-rich, PtSi, phase form. The sequential nature of the phase growth is directly related to the reduced thickness of the thin film (∼100 nm) and the interfacial reaction kinetics which limit the ability of multiple phases to grow.[2] The structure and composition of the interfacial region which dictates the growth sequence is poorly understood.

In contrast to the method described above, the deposition of semiconductors on metal surfaces by chemical vapor deposition (CVD) has received a relatively small amount of attention.[17−27] This omission may be of significant concern for device fabrication if wholly CVD-based processes were to be required for intermetallic thin-film growth. In addition to the applications in the semiconductor industry, semiconductor-modified metal surfaces have interesting implications in the area of catalysis. The electronic and structural modification of metal catalyst surfaces has yielded vast improvements in catalyst attributes (e.g., their activity, robustness, and selectivity).[18,28] In this study, the structure−reactivity relationships of a Pt(111) surface and its annealed Pt−Si overlayer were examined to explore the nature of the growth, physical, and chemical properties of Pt−Si intermetallic thin films.

We present the results of our initial studies of the reactions occurring between Si deposited by the surface-mediated decomposition of silane (SiH_4) on a Pt(111) surface. Auger electron spectroscopy (AES), low-energy electron diffraction (LEED), reflection−absorption infrared spectroscopy (RAIRS), and temperature-programmed desorption (TPD) were used in the present study to further the understanding of the structural and chemical properties of the resulting silicon-modified Pt(111) surface. The data indicate that annealing the deposited silicon results in the sequential growth of at least two intermetallic silicide thin films exhibiting long-ranged order. The sequential nucleation and growth of these unique structures resemble the structural changes observed for Pt thin films deposited on silicon substrates. Using chemisorbed CO as a probe of the surface reactivity, we also show that the structural and electronic modification of the Pt(111) surface by the silicon atoms in the intermetallic surface phase leads to large perturbations of the surface binding properties. This article will be

† Current address: Intel Corporation, Portland Technology Development, Hillsboro, OR 97214.

‡ Current address: Department of Chemistry, University of North Carolina at Chapel Hill, Chapel Hill, NC 27599.

S1089-5647(98)01398-4 CCC: $15.00
Published on Web 07/17/1998

followed by a detailed structural study of the morphological and compositional dependence of these and similarly prepared multilayer thin films using scanning tunneling microscopy (STM) and Auger electron spectroscopy.[29]

Experimental Section

The experiments discussed in this paper were performed in two ultrahigh-vacuum chambers (UHV), each with a working base pressure of $<3 \times 10^{-10}$ Torr. One was equipped with low-energy electron diffraction (LEED) optics (Physical Electronics). The second chamber was equipped with a differentially pumped (via a 45 L/s ion pump) Vacuum Generators SXP 300 mass spectrometer for TPD experiments and was interfaced with a Digilab FTS-60A spectrometer for RAIRS measurements. Each system also contained a single-pass cylindrical mirror analyzer (Physical Electronics) for Auger electron spectroscopy (AES) and sputtering guns for sample cleaning.

The Pt(111) crystal (Cornell Laboratories) was oriented to within 0.5° and polished using standard metallographic techniques. The Pt surface was cleaned with at least one cycle of Ar ion sputtering at 950 K for ∼15 min and annealing at 1050 K for 15 min. Surface cleanliness was established by AES (detectable carbon and oxygen <0.5 at. %). The crystal was heated with a button heater (Spectra Mat), and cooling was accomplished by connecting the crystal to a liquid nitrogen reservoir either by a copper braid or by direct thermal contact via the sample mount. A chromel/alumel (Omega) thermocouple attached directly to the side of the crystal allowed temperature measurement over the crystal operating temperature range of 90−1100 K. Silane (3% in UHP Ar, Matheson) was used as received and dosed from the background. Because large doses of Ar/silane mixture were used (due to the high dilution), the silane exposures reported throughout the paper are, at best, estimates. Carbon monoxide (Matheson) was dosed via an effusive molecular beam doser. The exposures used (monitored via the background gas load) were converted to coverages (fraction of θ_{sat}) by integrating the available TPD traces for CO dosing experiments and subsequently normalizing against the limiting exposure needed to saturate the surface with CO (θ_{sat}). These coverage values are, thus, approximate.

The reflection−absorption infrared (RAIR) spectra were collected using a broad-band, liquid nitrogen cooled, MCT detector. Reflection optics (∼*f*/12) were at near grazing angles of incidence with respect to the crystal surface normal (∼84°). Each RAIR spectrum represents 1024 scans taken at 4 cm^{-1} resolution, requiring a total collection time of ∼6 min (20 kHz modulation), and is presented as an absorbance plot ($-\log[R/R_0]$). The background spectra were collected from the clean surface prior to treatment of the Pt−Si surface with CO.

Temperature-programmed desorption (TPD) spectra were collected using a constant heating rate of 2 K/s. The spectra were measured using a Vacuum Generators SXP-300 mass spectrometer. The mass spectrometer was isolated by an enclosed Ni aperture (Beam Dynamics, Minneapolis, MN) which served both to shield the ionizer region of the mass spectrometer and to define the solid acceptance angle of the desorbing fragments. The latter feature allowed only species desorbing directly off the Pt(111) surface to be detected by the mass spectrometer.

Results

Auger Electron Spectroscopy. Changes in the composition of the Pt(111) surface were characterized after saturation (400 langmuirs) exposures to silane and various annealing treatments using Auger electron spectroscopy (AES). For demonstration, Figure 1 displays an AES spectrum for a clean Pt(111) surface compared with representative spectra of two $PtSi_x$ phases. On the clean Pt(111) surface, an intense peak is observed at 64 eV with an adjacent and significantly less intense peak at ∼92 eV. After the introduction of silicon onto the surface (as described in detail below), a peak at ∼92 eV, due to the silicon LMM Auger transition, is observed. The relative Si/Pt surface composition was calculated by ratioing the peak-to-peak distances for the low-energy Si and Pt Auger features found at 64 and 92 eV, respectively. This value is hereafter referred to as the AES Si/Pt ratio (*x* in $PtSi_x$). The two ordered silicide phases whose spectra are shown in Figure 1 are estimated by this method to have Si/Pt ratios of 0.29 and 0.52. These values are not corrected for the AES sensitivity factors. We note that the determination of absolute Si surface compositions is complicated by the overlap of the Pt and Si peaks at ∼92 eV in addition to the complications of the electronic structure which leads to the splitting of the Si peak in the high-coverage phase.[24] Because of this, only the relative changes in the Si and Pt surface composition were used to characterize the evolution of the surface composition during various thermal treatments.

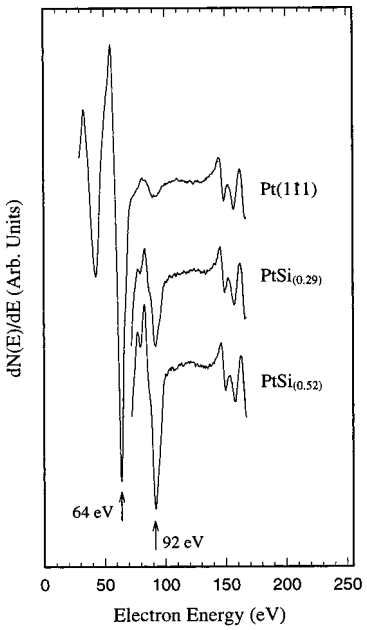

Figure 1. Representative Auger spectra for the clean Pt(111) surface and two representative silicide phases, $PtSi_{(0.52)}$ and $PtSi_{(0.29)}$, where *x* in $PtSi_x$ is the AES ratio for that phase. The Pt(111) spectrum was measured after sputtering and annealing the surface. After dosing a saturation coverage of SiH_4 on the surface at 275 K, the crystal was flash annealed to 750 and 950 K to form the $PtSi_{(0.52)}$ and $PtSi_{(0.29)}$ phases, respectively. The Si(92 eV)/Pt(64 eV) ratios were determined by ratioing the peak-to-peak distances for the respective low-energy peaks.

The temperature dependence of the reactive sticking probability of silane on the Pt(111) surface was determined qualitatively by measuring the Si/Pt ratio obtained after limiting doses of silane (∼400 langmuirs) were introduced at various surface temperatures. The Si/Pt ratio was found to be ∼0.2 at a deposition temperature of 110 K, indicating that dissociative chemisorption of silane was facile at 110 K. These results clearly owe to the mediation of the Si−H bond cleavage by the platinum surface.[25] A maximum Si/Pt value of ∼0.8 was measured when the silane was dosed on the Pt surface at ∼275 K while higher substrate temperatures resulted in the subsequent reduction of the measured AES ratio.

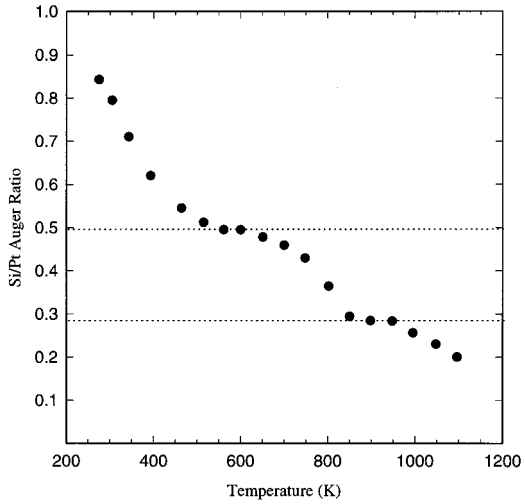

Figure 2. Evolution of the Auger spectra measured after sequentially flash annealing a silicon-saturated Pt(111) surface to increasing temperatures. The saturation coverage was achieved by dosing 400 langmuirs of silane at 275 K. The dashed horizontal lines are positioned to indicate the areas where the presented curve's slope is zero.

The strong sensitivity of the silicon uptake to the surface temperature is similar to that noted in previous studies of the dissociative chemisorption of silane on transition-metal surfaces where it was found that the reaction yields surface bound silyl species, SiH_x (where $0 < x < 4$), and adsorbed hydrogen at temperatures greater than 100 K.[17,18,24,25] For example, the silicon surface coverage on Cu(111) is 3 times larger for a saturation exposure of silane made at 300 K than is found at 100 K.[24] This temperature dependence was found to be strongly dependent on site blocking by the coadsorbed hydrogen atoms rather than the energetics of the Si−H bond rupture. Thus, silane deposition at temperatures where hydrogen recombination and desorption are facile (>250 K) affords higher silicon coverages simply as a result of the larger fraction of adsorption sites that are available. A similar restriction of the dissociative adsorption of silane occurs on the Pt(111) surface since the Si−H bond is easily activated by Pt at temperatures as low as 100 K.[25] The lower AES ratios determined for exposures made at temperatures above 275 K are misleading given that the interdiffusion of the Si atoms within the near-surface boundary layer is weakly activated (see below).

After preparing a saturation coverage silicon thin film (Si/Pt ~ 0.8) at 275 K, further heating in the absence of silane resulted in the reduction of the Si/Pt ratio. TPD studies, which detected no desorbing species other than H_2, confirmed that this change in the surface Si composition can only result from the interdiffusion of Si into the Pt crystal. This interdiffusion was examined by sequentially performing cycles of annealing and cooling of a Pt(111) crystal that had been initially exposed to 400 langmuirs of silane. In this process the crystal is heated to a specified temperature at a rate of 4 K/s followed by immediate cooling to 100 K (the cooling rate is an exponential function of temperature and has an average value of ~1 K/s) at which time AES was performed.[30] This process is then repeated, but with the annealing cycle being carried to a higher temperature and without cleaning the crystal between anneals. The compositional data as a function of the maximum annealing temperature are shown in Figure 2. The functional form of the compositional changes observed upon annealing vary sensitively with the thermal history and, thus, with the sample and the heating and cooling algorithm employed. We found that AES ratios calculated after flash anneals to a specific temperature (such as those found in Figure 2) are highly reproducible, having a range of only about 0.03 over several experiments. We emphasize for the reader, though, that the morphologies and compositions that are achieved as a result of these sequential anneals are not the same as those that would be found as a result of flash annealing to the corresponding maximum temperature (with no prior annealing treatments). *Such sensitivities are in fact expected for bimetallic phases formed via solid−solid interdiffusion processes which exhibit a time−temperature−transformation relationship.*[31] Interestingly, the Si dissolution process slows at 550 K and retains the ~0.5 AES ratio until ~650 K where the dissolution again becomes facile. A similar slope reduction is seen at ~850 K, corresponding to a Si/Pt composition of ~0.3. These apparent plateaus in interdiffusion kinetics indicate that there is a change in the activation barrier necessary for further dissolution of silicon into the Pt bulk at certain discrete compositions. For future discussion we will label these phases as $PtSi_{(0.52)}$ and $PtSi_{(0.29)}$. It is interesting to note that the stoichiometries observed at the plateaus mirror the evolution of the thin-film compositions formed from the interdiffusion of Si with excess Pt in the thin-film studies described by Ottaviani.[7] In these latter reactions which yield intermetallic films that are much thicker than those examined here, Pt_2Si is initially formed, and Pt_3Si only grows as the available silicon is depleted.

Low-Energy Electron Diffraction. Low-energy electron diffraction (LEED) was employed to look for the formation of overlayer phases possessing long-ranged order following deposition and annealing treatments. The evolution of the LEED patterns seen during the reaction of the deposited Si and the Pt(111) surface is shown in Figure 3 as a function of the AES Si/Pt ratio. Each pattern was recorded after annealing the Si/Pt(111) interface to the given temperature and subsequently cooling the sample to 100 K.

For reference, the first panel (Figure 3a) displays the (1 × 1) LEED pattern of the Pt(111) surface before dosing silane. After a saturation exposure to silane was effected at 275 K and the sample was cooled to 100 K, we found the (1 × 1) pattern had disappeared, indicating that the surface silicon overlayer may be disordered. Faint LEED spots became evident (Figure 3b) after flash annealing the sample to 600 K (giving a Si/Pt ratio of ca. 0.6). These new spots reflect the nucleation and growth of ordered domains which we assign to an intermetallic silicide thin film because the annealing temperature was sufficient to desorb all hydrogen (~350 K) from the Pt surface and promote some degree of interdiffusion (as evidenced by the AES data). The intensity and sharpness of the LEED pattern increased when a Si/Pt ratio of ~0.5 was obtained by flash annealing to 800 K.[32] The resulting pattern, which is best assigned to a $(\sqrt{7} \times \sqrt{7})R19.1°$ real space unit cell[33] (Figure 3c), is show schematically in Figure 3. The $\sqrt{7}$ LEED pattern persisted until a Si/Pt ratio of ~0.4 was obtained (via an additional anneal where the temperature was held at 800 K for 1 min; Figure 3d). This pattern was characterized by diffuse streaks which formed at the expense of the $\sqrt{7}$ pattern. The streaks intensified and were accompanied by the appearance of new, sharp spots after a Si/Pt ratio of 0.30 (flash anneal to 900 K) was reached. The nature of this streaky pattern is not completely understood. We believe that it may result from the partitioning of the overlayer between smaller (and degrading) $\sqrt{7}$ domains and a distinctly different structure (see below). The final LEED pattern, which became strikingly sharp and intense when a Si/Pt ratio of 0.25 was reached (after a flash anneal to 1050 K), is assigned to a $(\sqrt{19} \times \sqrt{19})R23.4°$ structure. The

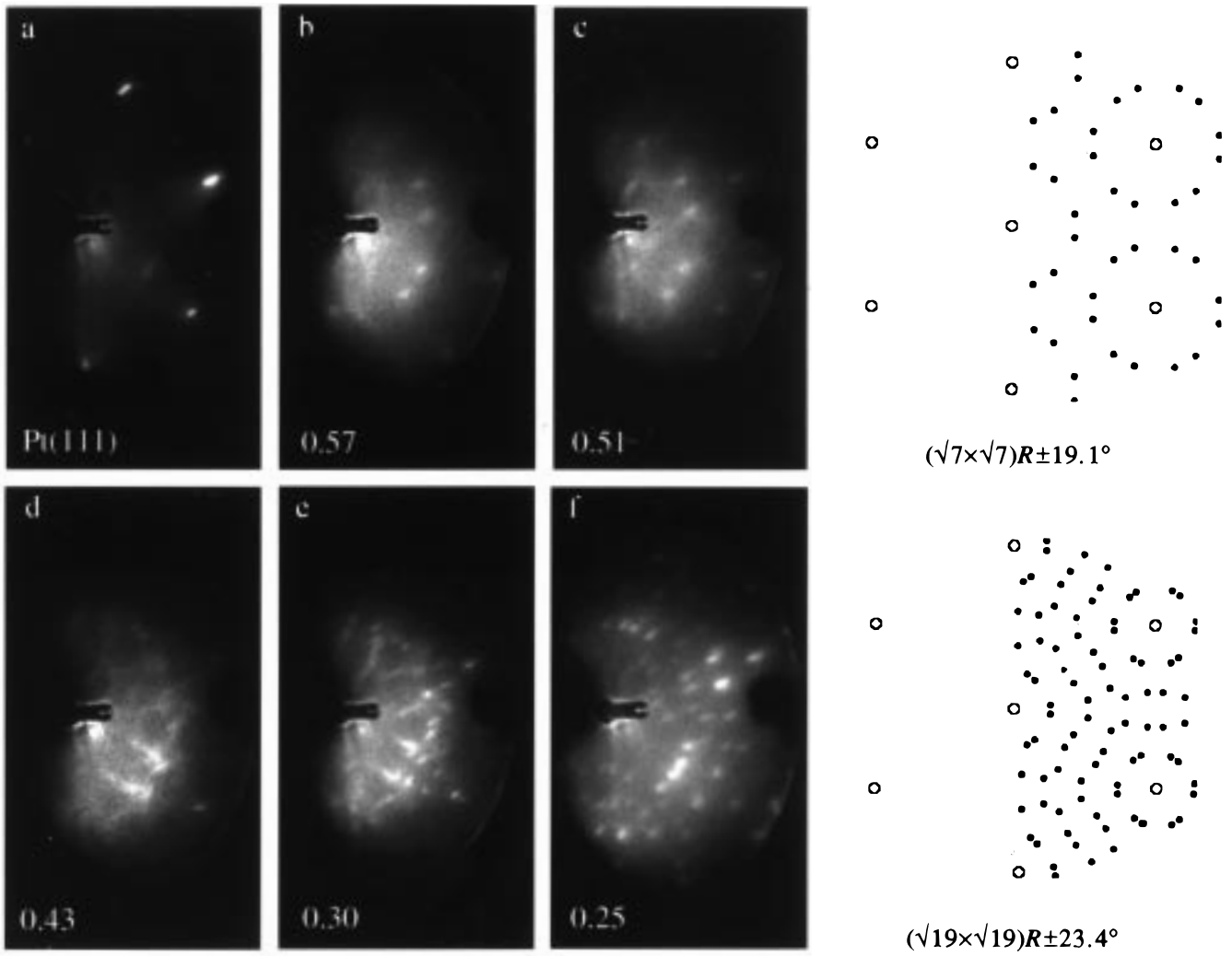

Figure 3. Low-energy electron diffraction (LEED) patterns measured at 100 K (beam energy 73 eV) from the (a) clean Pt(111) surface and (b−f) from silicide phases prepared by dosing a saturation coverage of Si at 275 K and then annealing. The right panel shows the schematic LEED patterns which result from the $(\sqrt{7} \times \sqrt{7})R19.1°$ and $(\sqrt{19} \times \sqrt{19})R23.4°$ real-space unit cells which were assigned to the patterns in (c) and (f), respectively. The LEED optics in this chamber are viewed at an off-normal angle.

$\sqrt{19}$ pattern was stable even after holding the crystal at 1100 K for short periods of time. Maintaining the crystal at 1100 K for several minutes, however, resulted in a diminished brightness and definition of the $\sqrt{19}$ spots. The assignment of these LEED patterns to $\sqrt{7}$ and $\sqrt{19}$ overlayers has been confirmed by detailed STM studies of platinum silicide thin-film growth and will be published separately.[29] A representative STM image (of the $\sqrt{7}$ phase) is provided in the Supporting Information. It is important to note that the two ordered LEED patterns occur at locations that are at or slightly higher than the temperatures corresponding to the "stability" plateaus seen in the AES data (Figure 2).

Reflection−Absorption Infrared Spectroscopy of Chemisorbed CO. RAIR spectra were measured after dosing CO onto the ordered platinum silicide surfaces and compared with those obtained on a clean Pt(111) substrate. On Pt(111), CO molecules adsorb normal to the surface plane via Pt−C bonds.[34] This surface bonding mode has been extensively explored by vibrational spectroscopies in part because the sensitivity of the CO stretching frequency to the adsorption site often allows the occupation of the atop, bridge, or 3-fold hollow sites to be determined by inspection of the spectra.[34] The intensities and frequencies of these bonding modes will, however, show strong coverage dependencies because the ordered CO monolayer behaves as a strongly coupled system rather than as independent dipole oscillators.[34−38]

For reference, Figure 4 displays the relevant RAIRS stretching bands measured after dosing increasing quantities of CO onto the Pt(111) surface at 100 K. This figure shows representative RAIR spectra for CO exposures which bracket significant coverage-dependent changes in the CO stretching frequencies on the clean and silicon-modified Pt surfaces. The coverages cited in the figure are normalized to that of a saturation coverage (see Experimental Section). The relative peak intensities and positions of the bands appearing in the data shown in Figure 4 are all consistent with the reported results of previous studies.[34−38] At low CO surface coverages ($\theta \approx 0.3\theta_{sat}$), a single absorption band is observed at 2088 cm^{-1}. This band is assigned to CO molecules bonded linearly and only to "atop" sites.[34] At higher coverages (e.g., $\theta \approx 0.7\theta_{sat}$, middle trace in Figure 4) an additional broad and less intense band due to CO bound at bridging sites is observed at ∼1820 cm^{-1}. This band sharpens and becomes more intense as the coverage is further increased (upper trace in Figure 4; $\theta \approx 0.8\theta_{sat}$), with the main peak shifting to ∼1850 cm^{-1} and an additional shoulder appearing at ∼1867 cm^{-1}. The frequency of the atop absorption band increases steadily with coverage to a maximum value of ∼2100 cm^{-1} after a saturation exposure to CO. The shift of this band to

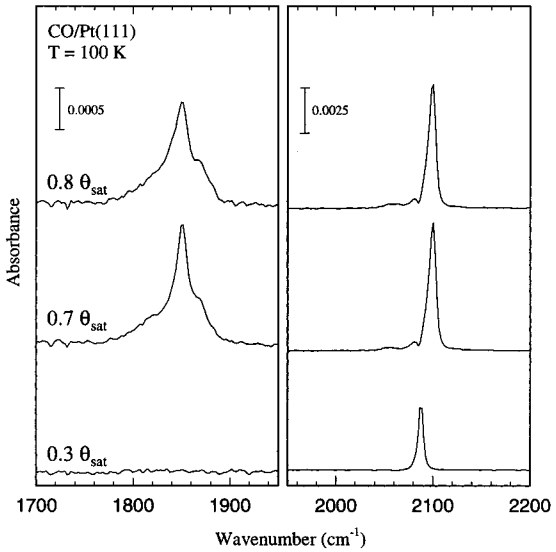

Figure 4. Reflection−absorption infrared spectra (RAIRS) taken after dosing the Pt−Si surface with a quantity of CO at 100 K sufficient to give the indicated coverage.

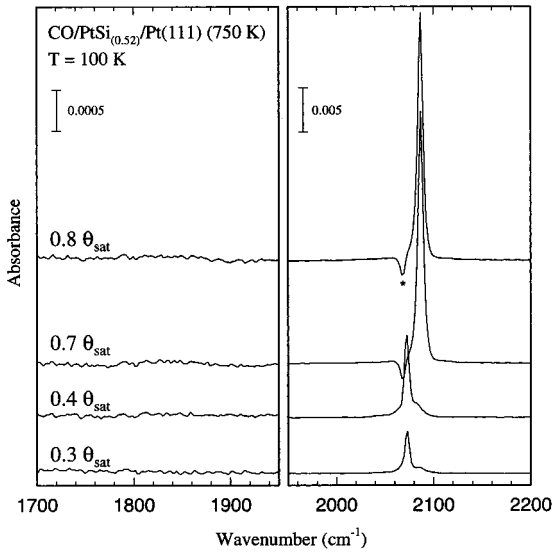

Figure 5. Reflection−absorption infrared spectra taken after dosing the indicated exposure of CO onto a $PtSi_{(0.52)}$/Pt(111) surface. The surface was prepared by dosing 400 langmuirs of silane at 275 K and flash annealing to 750 K, forming a Si/Pt auger ration of 0.52. The small negative peak (*) results from the adsorption of a small fraction of background CO while measuring the reference spectrum.

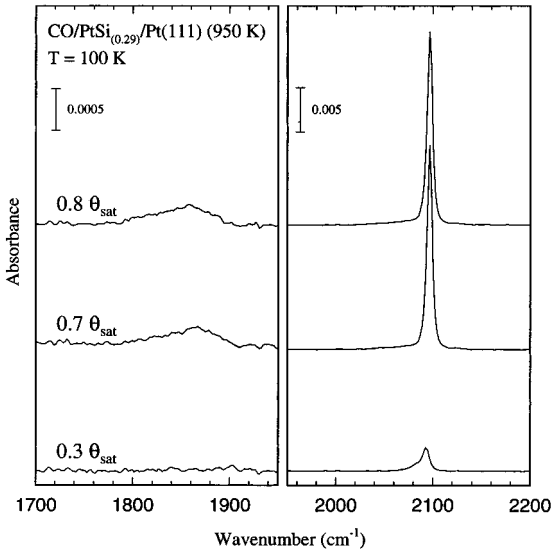

Figure 6. Reflection−absorption infrared spectra taken after dosing the indicated quantity of CO onto a $PtSi_{(0.29)}$/Pt(111) surface. The surface was prepared by dosing 400 langmuirs of silane at 275 K and flash annealing to 950 K, forming a Si/Pt Auger ration of 0.29.

higher frequency arises because of dipole−dipole coupling between the of CO molecules in an ordered overlayer.[34] The adsorbed CO molecules possess a large dynamic dipole moment whose coupling is known to give coverage-dependent shifts of as large as 18 cm^{-1}. A small frequency shift, which is related to the coverage-dependent changes in the Pt−C bonding, also contributes. Similar shifts have also been observed in the bands for molecules binding to bridging and 3-fold hollow sites.[34] The features of very low intensity observed at slightly lower frequencies than the atop band are ascribed to defect binding possibly as a result of CO islanding.[39]

In the RAIR spectra, the intense and easily resolved features of the CO vibrational spectrum provide a convenient means with which to make a determination of the binding sites adopted by the CO molecules on the Pt(111) surface. The spectra shown in Figure 4 can be correlated with the coverage-dependent phase diagram of the CO/Pt(111) adsorbate system, where studies have demonstrated several limiting adlayer structures. Briefly, they correspond to the formation of a low-coverage $(\sqrt{3} \times \sqrt{3})$-$R30°$ structure ($\theta_{CO} = 0.33$ where θ_{CO} is the coverage of CO relative to Pt(111)) where CO is bound to only atop sites. At higher CO coverages ($\theta_{CO} = 0.5$), the $\sqrt{3}$ structure compressed to a $c(4 \times 2)$ overlayer where about 50% of the CO molecules are forced to bridging sites because of surface crowding. Finally, at saturation coverages ($\theta_{CO} \sim 0.6$) compression structures are formed which are generally thought to possess only short-ranged order.[40,41]

In a typical RAIRS experiment on a silicide-modified substrate, the ordered phase of interest was prepared by annealing to the desired temperature and, subsequently, cooling the crystal to 100 K. Several (increasing) exposures of CO were then introduced into the chamber and the RAIR spectra measured. Figures 5 and 6 display the coverage dependence of the CO stretching modes seen on the $PtSi_{(0.52)}$ and $PtSi_{(0.29)}$ (i.e., the $\sqrt{7}$ and $\sqrt{19}$) structures formed by flash annealing a silane-dosed crystal to 750 and 950 K, respectively. We note that LEED did not reveal an ordering of the CO molecules bound to the silicides at 100 K for either phase.

A lower coverage CO overlayer ($\theta \approx 0.3\theta_{sat}$) on the $PtSi_{(0.52)}$ surface shows a single CO band at 2071 cm^{-1} with a small shoulder appearing at ~2083 cm^{-1} (Figure 5). Higher coverages ($\theta \geq 0.7\theta_{sat}$) resulted in an increase in both the intensity and frequency of this CO "atop" stretching band (with ν_{CO} shifting to 2087 cm^{-1}).[42] The CO coverage-dependent frequency shift of the atop band seen on the silicide surface was similar in magnitude to that observed on the clean surface but differing in its absolute intensity (see below). Perhaps the most significant aspect to note in the above spectra is the complete lack of a low-frequency adsorption band (~1850 cm^{-1}) at higher coverages which would be indicative of the formation of a significant population of bridge-bound CO. This suggests a significant change (from Pt(111)) in the available adsorption sites for CO due to the presence of Si (but not necessarily the complete lack of bridge-bound CO). Taken together, the data (AES, LEED, and RAIRS) suggest that the CO binds to a relatively homogeneous site population on the $PtSi_{(0.52)}$ surface (one exhibiting a well-defined $(\sqrt{7} \times \sqrt{7})R19.1°$ adlayer structure). It is certainly possible that there may exist a very

limited population of bridge-bound CO on this surface and for which the intensity in these spectra the low-frequency mode lies beneath the noise. Though the optical constants for this adsorbate system are not precisely known, it is reasonable that the transition magnitude of a CO bound to a bridge site on the intermetallic would not be vastly different from that characterizing the adsorbate on an atop site. With this assumption, the data suggest that only a small fraction of CO could possibly be bridge-bound and still remain undetectable by RAIRS. This profile (in which bridge site binding is relatively unimportant) suggests that only Pt or Si sites (but not both) bind this CO. We believe that the binding involves predominantly the Pt sites for the reasons discussed below.

In direct contrast to Pt, little is known about the adsorption of CO onto Si surfaces as very few studies have been reported.[43−45] HREELS studies suggest that CO does not bind to a defect-free Si(111)-(7 × 7) surface at 100 K but will adsorb onto a highly defective Si(111)-(7 × 7) substrate. This adsorbate does readily bind, however, to Si(100)-(2 × 1) at temperatures less than 220 K through the Si dimer pairs; the stretching frequency of this bound form of CO occurs at ∼2081 cm^{-1} (the value for gas-phase CO is 2065 cm^{-1}).[43] Additionally, Si is known to adsorb onto amorphous Si at 100 K with this bound state characterized by a very high vibrational frequency of 2104 cm^{-1}.[44,45] The Si−CO bond strength is weak in essentially all cases. The Si sites present in the $\sqrt{7}$ structure are, collectively, a well-defined structural population, and therefore, the binding of CO to Si (or Pt) defect sites (at more than nominal amounts) appears to be very unlikely. Comparisons with the Pt(111) reference spectra and literature data for Si suggest that both elements could serve as the binding site for the atop CO. (The frequencies for Si−CO and for atop Pt−CO are very similar, and thus, on this basis alone one cannot differentiate between them.) If CO were binding to a manyfold site (either Pt multiple, Si multiple, or jointly to Pt and Si), we also would expect to see a vibrational feature for bridge bonding at high CO exposures which we do not observe. Therefore, this is not a possibility. The most persuasive argument about the site involved (Si or Pt) comes from the TPD data (see below) which shows a binding enthalpy (albeit weakened) which is closer to that seen for atop Pt bonding than for single Si bonding. Structural arguments given below also suggest this bonding argument.

The RAIR spectra measured for CO overlayers on the $PtSi_{(0.29)}$ phase are shown in Figure 6. These spectra are similar to those measured for the $PtSi_{(0.52)}$ phase except that, at the lowest coverages, the CO stretching frequency is found to occur at 2093 cm^{-1} and higher CO coverages lead to only a small shift in band position to 2097 cm^{-1}. This shift of the atop band is significantly smaller (4 cm^{-1}) than the shift observed on either the clean Pt(111) surface (12 cm^{-1}) or the $PtSi_{(0.52)}$ phase (16 cm^{-1}) for a comparable range of coverages. As before, these data appear to be best described by a model in which the binding of CO occurs upon single Pt atom sites. At the highest coverages of CO, we also observe a broad and low-intensity peak centered at ∼1858 cm^{-1} which is unambiguously assigned to binding at multiple (presumably Pt) sites. This peak, when present, is significantly lower in intensity than the peak seen for the corresponding bridge-site bands for CO on the Pt(111) surface. The broad line width of this band suggests that it may correlate with a heterogeneous population of bonding structures (and possibly surface sites as well). We note that this latter feature may be due (at least, in part) to the binding of CO to adlayer defect sites.

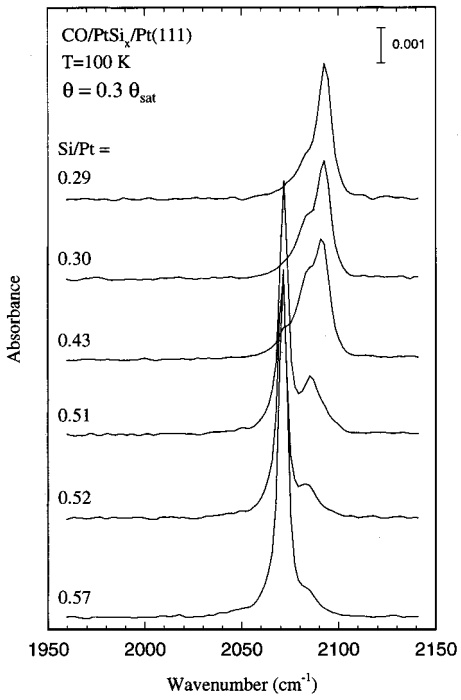

Figure 7. Reflection−absorption infrared spectra taken after dosing 0.025 langmuir of CO onto the indicated $PtSi_x$/Pt(111) surface.

The LEED data described above reveal that thermal treatment of the sample results in a progressive conversion of the $\sqrt{7}$ structure into that of the $\sqrt{19}$ adlayer, presumably via an interdiffusion process. The nature of this transformation can also be examined spectroscopically by using CO as a local probe of the adsorption sites present on the surface. A striking illustration of the use of this technique to follow this thin-film phase transformation is provided by the data shown in Figure 7. The data in this figure show the atop stretching band, measured at a nearly constant (and low) CO coverage ($\theta \approx 0.3\theta_{sat}$), for surfaces that were subjected to increasing annealing temperatures (prior to CO exposure). The AES ratios are subtly correlated with the details of the phase transformations evidenced by either LEED or RAIRS (and, as shown below, by TPD as well). AES averages over a finite, albeit shallow, sampling depth. Relatively modest atom motions can, therefore, greatly change surface site characteristics and may be difficult to discern by this method. Chemisorption properties, however, would be expected to respond much more sensitively to these motions. Conventional LEED analysis is also complicated by the difficulties presented by the identification of a small, incoherent fraction which might be involved in a progressive transformation mediated by a bulk (or near-surface) diffusion process. All the data, then, describe correlated aspects of the structural phase transformation which interconverts the two ordered adlayer structures identified in this work.

A sharp peak at 2071 cm^{-1} (with a weak shoulder) was observed on the $PtSi_{(0.57)}$ phase. At higher annealing temperatures sufficient to give Si/Pt ratios of 0.52 and (an essentially indistinguishable value of) 0.51, the shoulder centered at 2086 cm^{-1} grows in intensity without a shift in the position of the 2071 cm^{-1} peak. At a Si/Pt ratio of 0.43 there was a dramatic reduction seen in the intensity of the 2071 cm^{-1} peak, and spectra now show a pronounced new band at 2093 cm^{-1}. These changes are also accompanied by an increase in the intensity of the band centered at 2086 cm^{-1}. At a Si/Pt ratio of 0.30, the band at 2071 cm^{-1} has disappeared and the intensity of the peak at 2086 cm^{-1} has also declined markedly. Further heating

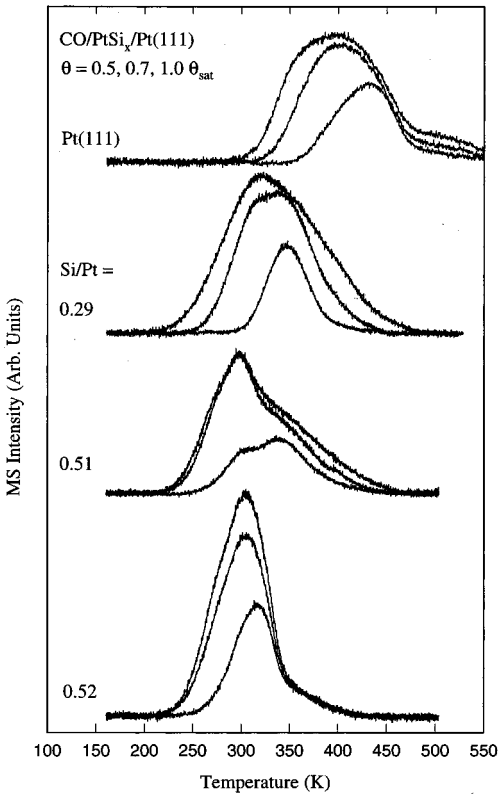

Figure 8. Temperature-programmed desorption (TPD) traces with detection of CO ($m/e = 28$) after the indicated doses of CO were introduced onto the $PtSi_{(0.52)}$ (750 K), $PtSi_{(0.51)}$ (800 K), $PtSi_{(0.29)}$ (950 K), and clean Pt(111) surfaces at 100 K.

to 950 K, which gave the $PtSi_{(0.29)}$ ($\sqrt{19}$) structure, showed a peak for a low coverage of CO at 2093 cm^{-1} with a very small shoulder still visible at ~2086 cm^{-1}.

The small differences seen in the CO stretching frequency as a function of the surface Si composition reflect changes in the electronic structure and the Pt adsorption sites present in each of the intermetallic phases. Thus, the frequency and coverage dependencies of this band provide a useful probe of the local structure of the available adsorption sites. By comparing the CO bands with the observed LEED patterns at each composition, a correlation can be made. A single peak at 2071 cm^{-1} is observed at the onset of the formation of the ordered $\sqrt{7}$ structure. The transition phase (Si/Pt ratio of 0.43) indicated by the "streaky" LEED patterns is coincident with the growth of a second peak at 2086 cm^{-1}. The distinct nature of this band provides evidence for the transitory presence of new adsorption sites (which may be due to defects, islanding, or both).[39] Finally, the presence of a single band at 2093 cm^{-1} correlates with the presence of the $\sqrt{19}$ LEED structure. We note that the relative intensities of CO bands, which are separated by less than 100 cm^{-1}, may show screening effects which result in intensity transfer from the low-frequency modes to the high-frequency modes.[52] Thus, the observed band intensities for the three modes described above should not be construed as reflecting the absolute concentrations of the identified adsorption sites. The spectra do provide a qualitative illustration of the sequential evolution in the surface structure and support the more general conclusions developed from LEED and AES.

Temperature-Programmed Desorption of CO. To obtain further insight into the energetics of the CO adsorption on the silicide phases, we carried out a series of coverage-dependent temperature-programmed desorption (TPD) studies. Figure 8 displays TPD traces measured for CO ($m/e = 28$) desorption after dosing the specified coverage of this adsorbate onto three silicide compositions at ~100 K. For reference, the top panel of Figure 8 shows the coverage dependence of the desorption of CO from a clean Pt(111) surface.

The desorption feature seen on Pt(111) at the lowest coverage is centered at ~430 K. This feature increases in intensity and shifts to ~395 K with increasing coverage. The trends seen in these data are consistent with previous results reported in the literature.[40] It is believed that the reduction seen in the desorption temperature as the surface coverage increases is related to a nearest-neighbor intermolecular repulsion in the adsorbed CO superstructure.

The desorption of CO from the $PtSi_{(0.52)}$ phase shows a narrow desorption feature with a maximum at ~315 K. Higher coverages result in a slight broadening and reduction in the desorption temperature to ~305 K and perhaps the formation a small shoulder on the low-temperature side. Interestingly, the fwhm of the high-coverage TPD trace is roughly half the value found for the corresponding trace for the Pt(111) surface. The reduction in the desorption temperature reveals that the heat of adsorption of CO is significantly lower on the silicide phases than on clean Pt(111). This result is consistent with electronic modification of the Pt sites by Si as it places the CO desorption region between that seen for Pt(111) and Si surfaces.[43] It is also consistent with the recently reported results of Wälchli et al. for evaporated Si on Pd(110).[44,45]

The low-coverage TPD trace from the silicide phase with a Si/Pt ratio of 0.51 (but annealed sufficiently to degrade the quality of the $\sqrt{7}$ LEED pattern) indicates the formation of two CO desorption peaks with maxima at ~295 and ~340 K. At higher coverages, the low-temperature peak grows in intensity and shifts to ~290 K while the high-temperature peak broadens. This complex desorption spectrum provides further evidence for the formation of a transitory ensemble of sites during the interconversion of the $\sqrt{7}$ and $\sqrt{19}$ structures as also indicated in the AES, LEED, and RAIRS studies.

After annealing the surface to 950 K, resulting in an AES Si/Pt ratio of 0.29, there is a significant shift in the temperature of the low-coverage CO desorption peak to ~350 K. This is indicative of a Pt-rich surface exhibiting a lesser electronic modification by Si. Larger exposures result in a more complex thermal desorption trace which is significantly broader. The maximum of the broad peak shifts to ~320 K. We believe that this complex line shape may reflect the presence of several CO chemisorption environments (and possibly distinct Pt sites) on this ordered surface structure. These sites may be the atop and bridge sites inferred from the RAIRS data. This latter structural correlation, though, is not completely persuasive given considerations of mass balance, and thus, these latter desorption kinetics remain poorly understood.

Discussion

The structure and chemical reactivity of chemically deposited silicon overlayers on a Pt(111) substrate were compared with the clean Pt surface. Independent results demonstrate that annealing the monolayer of surface-bound Si resulted in the consecutive formation and degradation of at least two unique thin-film silicide surface structures. The intermetallic structures form sequentially as the surface silicon diffuses from the surface into the bulk. The transformation mediated by this transport process demonstrates a pronounced time−temperature sensitivity. Each of these points will be discussed and compared with previously studied thin-film silicide interfacial reactions.

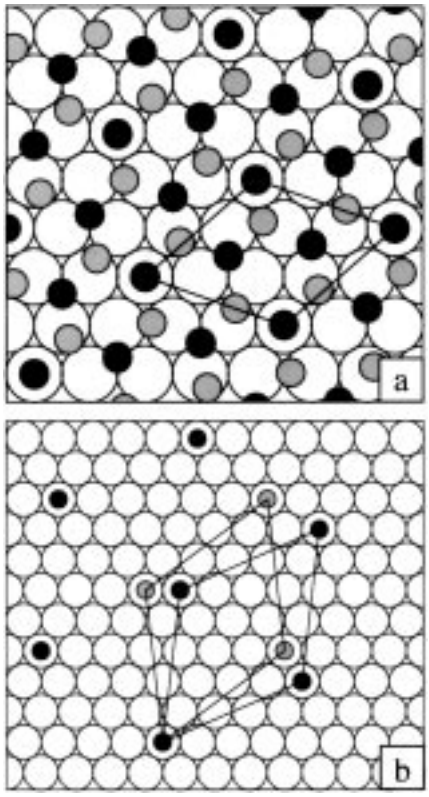

Figure 9. Schematic representations of overlayers which are consistent with the data presented in these studies for the $PtSi_{(0.52)}$ (a) and $PtSi_{(0.29)}$ (b) silicide phases. In (a) the overlayer is of the multilayer type with $(\sqrt{7} \times \sqrt{7})R19.1°$ symmetry and two types of species in two layers (black and gray), one of which corresponds to Si and the other to adlayer Pt. (b) is a adlayer (Si on Pt) of $(\sqrt{19} \times \sqrt{19})R23.4°$ symmetry. The two possible rotated domains for (b) are shown with different colored spots. Atop adlayer sites in the $\sqrt{19}$ overlayer are chosen simply for clarity. The identity of any additional subsurface layers cannot be inferred from these data.

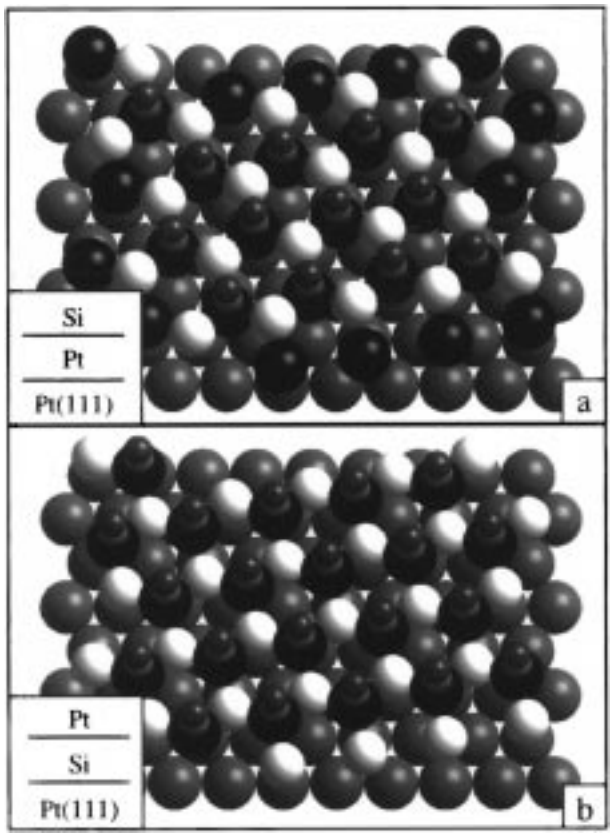

Figure 10. Hard-sphere representations of the adsorption of CO onto atop Pt sites which are part of the $(\sqrt{7} \times \sqrt{7})R19.1°$ overlayer for the cases where the Si atoms form the topmost layer (a) and the second layer (b). Si atoms are white and adlayer Pt atoms are black. In each case only those atoms that are wholly contained in an area defined by the selection of (111) substrate are shown, and the model is rotated 15° off-normal for clarity.

Flash annealing the saturated silicon surface overlayer to progressively higher temperatures results in a decrease in the measured surface silicon composition owing to the interdiffusion of the silicon into the Pt(111) substrate (Figure 2). The low kinetic energy of the AES peaks used in this analysis corresponds to mean free paths of ∼6 Å for these Auger electrons. The diffusion length probe here is, therefore, on the order of a few atomic diameters. The progressive decrease in the silicon surface composition with increasing annealing temperatures displays two apparent plateaus at Si/Pt AES ratios of ca. 0.5 and 0.3 (Figure 2). A similar sequential behavior was observed in the long-ranged ordering measured by LEED. Specifically, the two plateaus in the diffusion of silicon were observed at compositions near the formation of the ordered $(\sqrt{7} \times \sqrt{7})$-$R19.1°$ and $(\sqrt{19} \times \sqrt{19})R23.4°$ LEED patterns. Thus, the reduction in the rate of silicon interdiffusion into the bulk Pt must be related to the heat of reaction required to form each of these ordered surface phases. These formation temperatures are generally in accordance with the formation temperatures of platinum silicide thin-film phases (∼100 nm) grown by the diffusion of a vapor-deposited Pt film into a Si substrate. Specifically, Pt_2Si and Pt_3Si have been shown to form in the temperature range 473−773 K.[1]

On the basis of the results of our studies, we can propose a structure for the $\sqrt{7}$ overlayer (Figure 9a). This $\sqrt{7}$ structure is a bilayer structure which is very similar to that which has been described for copper sulfide thin films prepared on a Cu(111) surface[46] except that here one layer is adlayer Pt and the other Si (the grays and the blacks or vice versa). The alternative (and we believe naive) guess of a substitutional $\sqrt{7}$ structure is consistent with the AES and LEED data but has large numbers of multiple binding sites which would be freely accessible to CO. Our data do not support an argument that would require the bridge sites on such a structure to remain unoccupied at high CO coverages, and thus, we discount the importance of this simple structure. The proposed multilayer structure would be of the $\sqrt{7}$ type by LEED (secondary spots could easily be missed due to the low intensity and diffuse nature of the LEED pattern), has a Si coverage that is similar to the measured AES, and completely lacks multiple binding sites for CO (the same-layer interatom distance is 4.23 Å). In this way, it is consistent with all presented data. Data from STM studies, which we will report shortly in a separate paper, clearly argue in favor of a $\sqrt{7}$ structure with this corrugation and symmetry (see Supporting Information).[29]

Simple hard-sphere modeling of the CO bonding (Figure 10) atop to Pt in each potential variation of the $\sqrt{7}$ overlayer (the first or second levels) indicates that CO has sufficient space to bond to atop sites for atoms in either the first or second layers, and thus, the identity of which species (Si or Pt) terminates this structure remains unresolved. Using a simple site-blocking model, the $\sqrt{7}$ structure strongly suggested by LEED and STM data, as modeled in Figure 10, would have a CO occupancy of ∼71% with respect to saturation (again assuming only a single metal atom site is occupied on the Si−Pt surface).

A proposed structure for the adlayer giving the $\sqrt{19}$ LEED pattern is shown in Figure 9b. (Atop sites are chosen in this

figure for clarity only; we have no direct information on the actual site occupied by adatoms.) This schematic overlayer is of the simple substitutional type and, thus, is necessarily compatible with the LEED data. Significant aspects of this structure remain incompletely understood. In the AES studies for example, the Si/Pt ratio for this structure has a maximum value of 0.30 while the simplest version of the proposed overlayer requires 0.053 (calculated value) of a monolayer of Si to construct. The RAIRS data, further, do not suggest that a large number of multiple Pt binding sites are available while a simple substitutional $\sqrt{19}$ overlayer has many such sites. STM studies do, however, confirm the symmetry and physical size of this structure.[29] It must be recalled at this point that the true structural nature of this phase cannot be completely described by any simple substitutional or adlayer model.

The structural evolution of the Pt(111) surface to the $\sqrt{7}$ and the $\sqrt{19}$ overlayers reflects a sequential increase in the size of the hexagonal real-space surface unit cells. The increase of the unit cell size when proceeding from the $\sqrt{7}$ to the $\sqrt{19}$ structure is consistent with the reduction in the surface concentration of Si by AES. The most important point to note here, though, is that this evolution of surface unit cells must proceed via the redistribution of both Si and Pt in a thin (but not single) surface layer. There is, therefore, no doubt that the latter ($\sqrt{19}$) Pt−Si structure is more complex than that given in Figure 9b. The precise nature of this thin-film structure may not be resolved without a more detailed examination using appropriate diffraction methods. The formation of the large hexagonal surface unit cell structures in silicide thin films finds precedent in the literature. For example, Diebold et al. recently reported a $\sqrt{19}$ structure on the Pt(111) surface which resulted from the surface segregation of impurity Si (and perhaps Ca).[47] In addition, Morgen et al. found the formation of a $\sqrt{7}$ and ($\sqrt{3} \times \sqrt{3}$)-*R*30°structures for thin Pt films on Si(111).[10] These structures, however, were believed to be of a simple, substitutional type.

Our present understanding of the structure of the Si−Pt surfaces is not sufficient to completely describe the overlayer structures formed upon CO adsorption. The intensities seen in the RAIRS data, for example, are difficult to quantify given that electronic effects are prominent. In addition, ordered LEED patterns are not observed for these CO adlayers.

Further evidence for the reduced fraction of adsorption sites in the silicide phases was provided in the TPD studies. Specifically, the CO desorption line shapes obtained from the $PtSi_{(0.52)}$ surface were significantly narrower than those measured on the clean Pt surface at all coverages. This supports the reduction in the number of possible CO bonding sites due to the presence of the Si and is consistent with the presence of CO bonding at only atop sites (as shown by RAIRS) in a structure such as that shown in Figure 9a (see also Figure 10). A similar narrowing and reduction in the peak intensity has been found for the desorption of CO from Sn/Pt(111) surfaces.[48] The changes seen in that study were attributed to a modified precursor state due to the presence of the Sn atoms. We note that the change in the desorption temperature on the silicide phase was significantly larger than seen for the Pt−Sn surface. The CO desorption spectra obtained from the $PtSi_{(0.29)}$ phase also were narrower than that for the Pt surface at low CO coverages but only to a modest degree. At higher coverages, however, broad desorption features are seen on both. The presence of defect sites cannot be ruled out as contributing to the observed TPD behaviors especially since these sites are clearly indicated by the RAIRS studies (Figure 7).

The reduction in the heat of adsorption of the CO on the silicide thin film, as determined by TPD, reflects a significant decrease in the Pt−CO bond strength with respect to the clean Pt surface. Based on a simple Redhead analysis[49] which assumes first-order desorption kinetics and a preexponential factor of $\sim 10^{13}$ s^{-1}, the decrease in the low-coverage heat of adsorption is ~7 kcal/mol for the $\sqrt{7}$ and ~5 kcal/mol for the $\sqrt{19}$ structures. The RAIR spectra do not correlate with these differences in a simple way. As was discussed above, the frequencies of the atop CO band seen at low coverage for both silicide phases straddle the value found on the Pt surface. These results are not consistent with a general molecular orbital model of CO chemisorption on a transition-metal surface which suggests an inverse correlation between in the M−CO bond strength and the CO stretching frequency.[50−52] In this model, a strong M−CO bond results from strong metal donation to the 2π antibonding orbitals of the CO molecule. Population of the CO antibonding orbitals weakens the C−O bond and decreases the C−O stretching frequency. Because this general relationship is not obeyed on the silicide surface, there must be other factors that contribute to the CO stretching frequency, namely, Si electronic modification of the Pt−Si surface away from the Pt(111) ideal. Similar behavior has been observed on other modified transition-metal surfaces such as Cu/Pt(111) surfaces.[52] The nature of these perturbations is poorly understood.

Perhaps the most striking feature of these results is the structural evolution of the silicide phases, one which is consecutive in nature. This property may be characterized as the growth or dissolution of only a single structural phase at any given annealing temperature (or time as embodied in a time−temperature−transformation relationship). This was most evident in the LEED data wherein we observe the formation of the $\sqrt{7}$ structure followed by its dissolution to an intermediate state with a higher defect density followed by the formation of the $\sqrt{19}$ structure. Each of these phases must be characterized by a distinct (exothermic) heat of formation. Additional support for this transformation model was provided by the RAIRS data (shown in Figure 7) which displays the evolution of the low-coverage CO atop stretching frequency for several silicide structural types. These data demonstrate the consecutive growth of at least two distinct Pt−CO bonding sites, a result which again correlates well with the LEED and AES data.

The consecutive model of silicide thin-film growth has been extensively studied with regard to the formation of thin films via the reaction of metals deposited on silicon substrates.[1,2,5−8] Previous studies of thin platinum films (~100 nm) deposited on silicon indicate that, at annealing temperatures well below the lowest eutectic, Pt_2Si is formed uniformly at the interface. In the case where the quantity of silicon is limited, a second more platinum-rich phase, Pt_3Si, forms through depletion of the Si in the Pt_2Si phase.[6] Although the relationship between the thin-film phases prepared in this study and those in the thin-film reactions previously studied is unknown, it is clear that a similar pattern of consecutive evolution is present in this case as well. We note that the surface unit cells found in this study are inconsistent with the low index faces for all known bulk platinum silicide crystal structures.[53] Therefore, we cannot assign these surface structures to the familiar Pt_2Si and Pt_3Si phases. This latter aspect of the data suggests that the phase formation in the present system is strongly directed by the crystallographic characteristics of the underlying (111) orientation of the fcc Pt lattice structure. We will provide a more detailed examination of these structural issues in subsequent reports.

Acknowledgment. We are especially grateful to Helen Farrell for her help in the interpretation of the LEED data. This work was supported by the Department of Energy (DEFG02-91ER45439) through the University of Illinois Frederick Seitz Materials Research Laboratory and the National Science Foundation (CHE-9626871). M.S.N. and J.C.B. acknowledge financial support via fellowship awards from the Department of Chemistry and the NSF, respectively.

Supporting Information Available: A representative STM image of the $\sqrt{7}$ phase (1 page). Ordering information is given on any current masthead page.

References and Notes

(1) Tu, K. N.; Mayer, J. W. In *Thin Films-Interdiffusion and Reactions*; Tu, K. N., Mayer, J. W., Eds.; Wiley: New York, 1978; pp 359−405.

(2) Mayer, J. W.; Lau, S. S. In *Electronic Materials Science*: For Integrated Circuits in Si and GaAs; Mayer, J. W., Lau, S. S., Eds.; Macmillan: New York, 1990; pp 275−303.

(3) Muraka, S. P. *Silicides for VLSI Applications*; Academic Press: New York, 1993.

(4) Sandersreed, J. N. *Opt. Eng.* **1997**, *36*, 235−242.

(5) Ottaviani, G. *J. Vac. Sci. Technol.* **1979**, *16*, 1112−1118.

(6) Ottaviani, G. *J. Vac. Sci. Technol.* **1981**, *18*, 924−928.

(7) Canali, C.; Majni, G.; Ottaviani, G.; Celotti, G. *J. Appl. Phys.* **1979**, *50*, 255−258.

(8) Pretorius, R. *Thin Solid Films* **1996**, *290*−291, 477−484.

(9) Rossi, G. *Surf. Sci.* **1987**, *7*, 1−101.

(10) Morgen, P.; Szymonski, M.; Onsgaard, J.; Jørgensen, B. *Surf. Sci.* **1988**, *197*, 347−362.

(11) Itoh, H.; Narui, S.; Sayama, A.; Ichinokawa, T. *Phys. Rev. B* **1992**, *45*, 11136−11142.

(12) Das, S. R.; Sheergar, K.; Xu, D.-X.; Naem, A. *Thin Solid Films* **1994**, *253*, 467−472.

(13) Colgan, E. G. *J. Mater. Res.* **1995**, *10*, 1953−1957.

(14) Hsu, D. S. Y.; Troilo, L. M.; Turner, N. H.; Pierson, K. W. *Thin Solid Films* **1995**, *269*, 21−28.

(15) Ley, L.; Wang, Y.; Nguyen, V.; Fisson, S.; Souche, D.; Vuye, G.; Rivory, J. *Thin Solid Films* **1995**, *270*, 561−566.

(16) Lifshits, V. G.; Saranin, A. A.; Zotov, A. V. *Surface Phases on Silicon. Preparation, Structures, and Properties*; John Wiley & Sons: New York, 1994; pp 352−357.

(17) Dubois, L. H.; Zegarski, B. R. *Surf. Sci.* **1988**, *204*, 113−128.

(18) Dubois, L. H.; Nuzzo, R. G. *Surf. Sci.* **1985**, *149*, 133−145.

(19) Sault, A. G.; Goodman, D. W. *Surf. Sci.* **1990**, *235*, 28−46.

(20) Dubois, L. H.; Nuzzo, R. G. *Langmuir* **1985**, *1*, 663−669.

(21) McCash, E. M.; Chesters, M. A.; Gardner, P.; Parker, S. F. *Surf. Sci.* **1990**, *225*, 273−280.

(22) Dubois, L. H.; Nuzzo, R. G. *Surf. Sci.* **1985**, *149*, 119−132.

(23) Dubois, L. H.; Zegarski, B. R. *J. Vac. Sci. Technol. A* **1988**, *6*, 870−874.

(24) Wiegand, B. C.; Lohokare, S. P.; Nuzzo, R. G. *J. Phys. Chem.* **1993**, *97*, 11553−11562.

(25) Hostetler, M. J.; Nuzzo, R. G.; Girolami, G. S. *J. Am. Chem. Soc.* **1994**, *116*, 11608−11609.

(26) Lohokare, S. P.; Wiegand, B. C.; Nuzzo, R. G. *Langmuir* **1995**, *11*, 3902−3912.

(27) Kanazawa, T.; Kitajima, Y.; Yokiyama, T.; Yagi, S.; Imanishi, A. *Surf. Sci.* **1996**, *357*−358, 150−164.

(28) See for example: (a) Sinfelt, J. H. *Bimetallic Catalysts*—Discoveries, Concepts, and Applications; John Wiley & Sons: New York, 1983. (b) Anderson, J. R. *Structure of Metallic Catalysts*; Academic Press: New York, 1975. (c) Klabunde, K. J.; Li, Y.-X. *Selectivity in Catalysis*; Davis, M. E., Suib, S. L., Eds.; American Chemical Society: Washington, DC, 1993.

(29) Bondos, J. C.; Gewirth, A. A.; Nuzzo, R. G., to be submitted.

(30) We term this annealing treatment a flash anneal. This type of annealing treatment is the same type that is used throughout the paper unless otherwise noted in the text. Flash anneals mentioned in the text after those portrayed in Figure 2 are, however, not sequential. In these (latter) cases, a Si/Pt(111) surface is subjected to a flash anneal, analyzed, and then cleaned prior to the performance of a second anneal. It should be noted that if the annealing cycles are individual (not sequential), the resultant Auger ratios will be somewhat higher due to the lack of time spent at elevated temperatures prior to the point (annealing cycle) of interest. The magnitude of this effect tends to be greater for lower (but above room temperature) anneals.

(31) See for example: Burke, J. *The Kinetics of Phase Transformations in Metals*; Pergamon Press: New York, 1965; pp 58−60.

(32) Christmann, K.; Ertl, G.; Pignet, T. *Surf. Sci.* **1976**, *54*, 365−392.

(33) The geometry of our chamber unfortunately does not allow us to take rearview images. We present in Figure 3 the largest field of view that our camera can capture ($>^1/_2$ of the pattern) and note for the reader that the half of the pattern that is not visible is completely consistent with the portion shown.

(34) Bradshaw, A. M.; Schweizer, E. In *Infrared Reflection Absorption Spectroscopy of Adsorbed Molecules*; Hester, R. E., Ed.; John Wiley & Sons: New York, 1988; pp 413−483.

(35) Tüshaus, M.; Schweizer, E.; Hollins, P.; Bradshaw, A. M. *J. Electron Spectrosc. Relat. Phenom.* **1987**, *44*, 305−316.

(36) Ryberg, R. *Adv. Chem. Phys.* **1989**, *76*, 1−45.

(37) Malik, I. J.; Trenary, M. *Surf. Sci.* **1989**, *214*, L237−L245.

(38) Schweizer, E.; Persson, B. N. J.; Tüshaus, M.; Hoge, D.; Bradshaw, A. M. *Surf. Sci.* **1989**, *213*, 49−89.

(39) Hoge, D.; Tüshaus, M.; Bradshaw, A. M. *Surf. Sci.* **1988**, *207*, L935−L942.

(40) Ertl, G.; Neumann, M.; Streit, K. M. *Surf. Sci.* **1977**, *64*, 393−410.

(41) Steininger, H.; Lehwald, S.; Ibach, H. *Surf. Sci.* **1982**, *123*, 264−282.

(42) The weak negative intensity feature seen at a lower frequency than the main peak (* in Figure 5) is due to a small quantity of CO adsorbed from the background during the acquisition of the reference spectra. It is sufficiently weak that it will only nominally affect the high-coverage peak line shape or position measured in this experiment.

(43) Bu, Y.; Lin, M. C. *Surf. Sci.* **1993**, *298*, 94−100 and references therein.

(44) Wälchli, N.; Kampshoff, E.; Kern, K. *Surf. Sci.* **1996**, *368*, 258−263.

(45) Wälchli, N.; Kampshoff, E.; Menck, A.; Kern, K. *Surf. Sci.* **1997**, *382*, L705−L712.

(46) Prince, N. P.; Seymour, D. L.; Ashwin, M. J.; McConville, D. P.; Woodruff, D. P.; Jones, R. G. *Surf. Sci.* **1990**, *230*, 13.

(47) Diebold, U.; Zhang, L.; Anderson, J. F.; Mrozek, P. *J. Vac. Sci. Technol. A* **1996**, *14*, 1679−1683.

(48) Xu, C.; Koel, B. E. *Surf. Sci.* **1994**, *304*, L505.

(49) Redhead, P. A. *Vacuum* **1962**, *12*, 203.

(50) Cotton, F. A.; Wilkinson, G. *Advanced Inorganic Chemistry*, 5th ed.; John Wiley & Sons: New York, 1988.

(51) Toolenaar, F. J. C. M.; Reinalda, D.; Ponec, V. *J. Catal.* **1980**, *64*, 110−115.

(52) Rodriguez, J. A.; Goodman, D. W. *Science* **1992**, *257*, 897−1528.

(53) Villars, P.; Calvert, L. D. *Pearson's Handbook of Crystallographic Data for Intermetallic Phases*, 2nd ed.; ASM: Materials Park, 1991; Vol. 4, pp 4994−4995.